BCL-2 family proteins form distinct functional interaction networks when primed with full-length BAD compared with the BAD-like mimetic ABT-737.

Robert Pedley* [1,2,4], Charlotte E. L. Mellor* [1,2, 5], Louise E. King [1,2], Louisa Nelson[1,2], Fabianna Tennant[1,2], Matthew Jones[1 ,2], Isobel Taylor-Hearn[1,2], Alexander Mironov [3], Craig Lawless[1] and Andrew P. Gilmore[1,2#].

* * These authors contributed equally to this work. The order of joint first authors was determined by a coin flip.

Supplementary materials

Supplementary data figures

Figure S1. Bax retrotranslocation dependent mitochondrial interaction.

A. Venn diagram of gene lists derived from experiments described in Fig. 1C indicating limited overlap between predicted and observed interactions.

B. Schematic representation of BirA*-BaxWT and BirA*-BaxS184V subcellular localisation, retrotranslocation dynamics and predicted labelling patterns, with representation of BioID expression constructs.

C. Representative images of MCF10A cells stably expressing either BirA*-BaxWT, BirA*-BaxS184V or Venus-BirA*. Cells were fixed and immunostained for the indicated proteins (mtHSP70 and Myc-tag). Scale bar represents 10 μm.

D. Volcano plots of BioID SAINT analysis identified prey proteins significantly enriched by BirA*-BaxWT or BirA*-BaxS184V, relative to Venus-BirA* expressing cells.

E. Heatmap representation of the average protein intensity for significant prey proteins. The average protein intensity for preys that had a SAINT derived BFDR of <0.05 (Fig. S1D) are displayed for BirA*-BaxWT and BirA*-BaxS184V conditions. Data represent the mean of three independent experiments and are unscaled.

Figure S2. Proximity labelling identifies that Bcl-2 has a wider subcellular distribution than Bcl-XL.

A. MCF10A cell lysates from stable cell lines expressing Venus-BirA*, BirA*-Bcl-XL or BirA*-Bcl-2 immunoblotted with anti-Myc confirms equivalent expression levels of each bait. Anti-vinculin was used as a loading control.

B. Immunofluorescence imaging of the MCF10A lines in FigS2A. Fixed cells were immunostained with anti-mtHSP70 and anti-Myc-Tag, as indicated. Scale bar = 10 μm.

C. Venn diagram comparing the significant hits (BFDR < 0.05) in the Bcl-XL and Bcl-2 datasets. Prey proteins which are significant in both datasets are identified by the gene name.

D. Reactome analysis of significant preys identified in the BirA*-Bcl-2 and BirA*-Bcl-XL BioID analysis.

E. Analysis of the biological processes associated with the significantly enriched preys in the BirA*-Bcl-2 and BirA*-Bcl-XL BioID analysis.

Figure S3. The BirA*-Bcl-XL proximity interactome shows differential changes when cells are primed by either Bad or the Bad BH3-mimetic ABT-737.

A. Immunofluorescence staining of MCF10A cells stably expressing Venus-BirA* and BadER, and treated with DMSO, 10μM 4-OHT or 5μM ABT-737. In the left panel, cells were co-immunostained with anti-mtHSP70 and anti-myc tag, along with DAPI. Right panel - cells were co-immunostained for the ant-oestrogen receptor (ER) tag to show the BadER fusion protein, alongside anti-mtHSP70 and DAPI. Scale bar = 10μm.

B. Venn diagram summarising the overlap of significant BioID preys per condition from the BioID data in Fig. 4C.

C. Mapping of the Bcl-xL STRING-predicted interactions (dotted lines) alongside identified BioID hits from Fig. 4C.

D. MCF10A cells expressing BadER and GFP-Bcl-XL were subjected to fluorescence recovery after photobleaching (FRAP) analysis as described previously [7] and in the methods. FRAP experiments were carried out with cells treated with either DMSO, 10 μM 4-OHT or 5 μM ABT-737. Cells were photobleached within the region of interest (ROI) indicated by the yellow box, and imaged post-bleach recovery for 140 seconds.

Figure S4. The BirA*-Bcl-2 proximity interactome shows differential changes when cells are primed by either Bad or the Bad BH3-mimetic, ABT-737.

A: Top panel: Schematic representation of the expression constructs BirA*-Bcl-2 and BadER. Bottom panel: Immunoblots of whole cell lysates of each stable line, using anti-vinculin, anti-Myc-tag, and anti-ER, show similar expression of bait protein and BadER.

B. Left panel: Validation of stable MCF10A cells expressing BadER/BirA*-Bcl-2 and BadER/Venus-BirA*. Left panels: Immunofluorescence imaging of both lines with anti-mtHSP70 and anti-Myc-tag, following treatment with DMSO, 4-OHT or 5μM ABT-737. Scale bar is 10μm. Right panel: To validate function of BirA*-Bcl-2, MCF10A cells stably expressing BadER/BirA*-Bcl-2 were treated with DMSO, 10μM 4-OHT or 5μM ABT-737 with and without 800μM etoposide. Cells were cultured with FITC-Annexin V and PI and images were taken every hour for 18 hours. The number of Annexin V positive cells was counted as a percentage of the total initial cell population. Mean percentages of apoptosis over time are plotted from two independent experiments.

C. Volcano plots showing Significance Analysis of Interactome (SAINT) of BioID preys enriched in MCF10A cells expressing BirA*-Bcl-2 relative to Venus-BirA* expressing cells in each of three conditions: cell treated with DMSO; cell treated with 4-OHT to activate BadER; and cells treated with ABT-737. Significant preys (BFDR < 0.05) indicated in each condition.

D. Heatmap showing the relative enrichment of prey proteins across the DMSO, 4-OHT and ABT-737 conditions from Fig. S5C. Each prey is included where it reached the BFDR < 0.05 in a least one of the conditions.

Figure S5. Full-length Bad and the Bad mimetic ABT-737 have distinct effects on mammary epithelial cells.

A. Overrepresentation analysis of RNAseq data from MCF10A cells expressing BadER and BirA*- Bcl-XL following 18-hour DMSO, 4-OHT or ABT-737 treatment, based on biological processes.

B. Overrepresentation analysis of RNAseq data from MCF10A cells expressing BadER and BirA*- Bcl-XL following 18-hour DMSO, 4-OHT or ABT-737 treatment, based on reactome pathways.

C. Immunofluorescence staining of BadER-GFP BirA*-Bcl-xL MCF10A for pPERK and BiP following treatment with DMSO, 4-OHT, ABT-737 or thapsigargin, as described in the methods. Scale bar = 10 μm.

D. BadER-GFP-Bcl-xL MCF10A cells immunostained stained for anti-GFP and p62 following treatment with DMSO, 4-OHT, ABT-737 or CCCP, as indicated. Scale bar = 10 μm.

Figure S6. Full-length western blots.

For all full-length western blots, the cropped area shown in the main figure is indicated by the red box.

A. Full-length western blots for Figure 1B. Left-hand side shows the eluted material from the streptavidin pull-down for one biological replicate for Figure 1D. 1:10 of the eluted material was run on the blot.

B. Full-length western blot for Figure 3C.

C. Full-length western blot for Figure S2A.

D. Full-length western blot for Figure S4A.

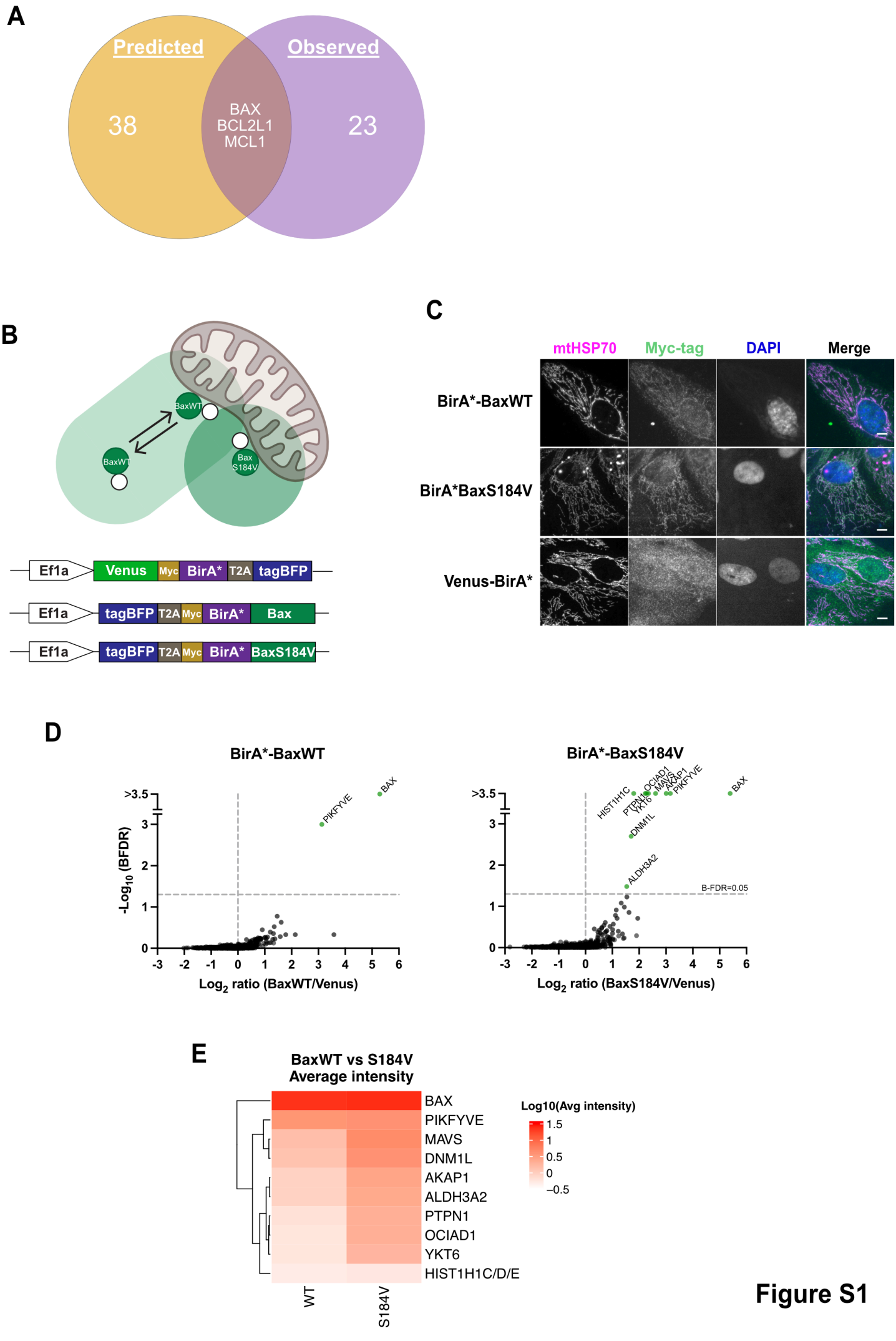
A
Predicted
Observed
38
BAX
BCL2L1
MCL1
23
B
BaxWT
BaxWT
Bax S184V
Ef1a
Venus
Myc
BirA*
T2A
tagBFP
Ef1a
tagBFP
T2A
Myc
BirA*
Bax
Ef1a
tagBFP
T2A
Myc
BirA*
BaxS184V
C
mtHSP70
Myc-tag
DAPI
Merge
BirA*-BaxWT
BirA*BaxS184V
Venus-BirA*
D
BirA*-BaxWT
BirA*-BaxS184V
-Log10 (BFDR)
Log2 ratio (BaxWT/Venus)
Log2 ratio (BaxS184V/Venus)
PIKFYVE
BAX
HIST1H1C
PTPN1
OCIAD1
YKT6
MAVS
AKAP1
DNM1L
ALDH3A2
B-FDR=0.05
E
BaxWT vs S184V
Average intensity
BAX
PIKFYVE
MAVS
DNM1L
AKAP1
ALDH3A2
PTPN1
OCIAD1
YKT6
HIST1H1C/D/E
WT
S184V
Log10(Avg intensity)

Figure S1

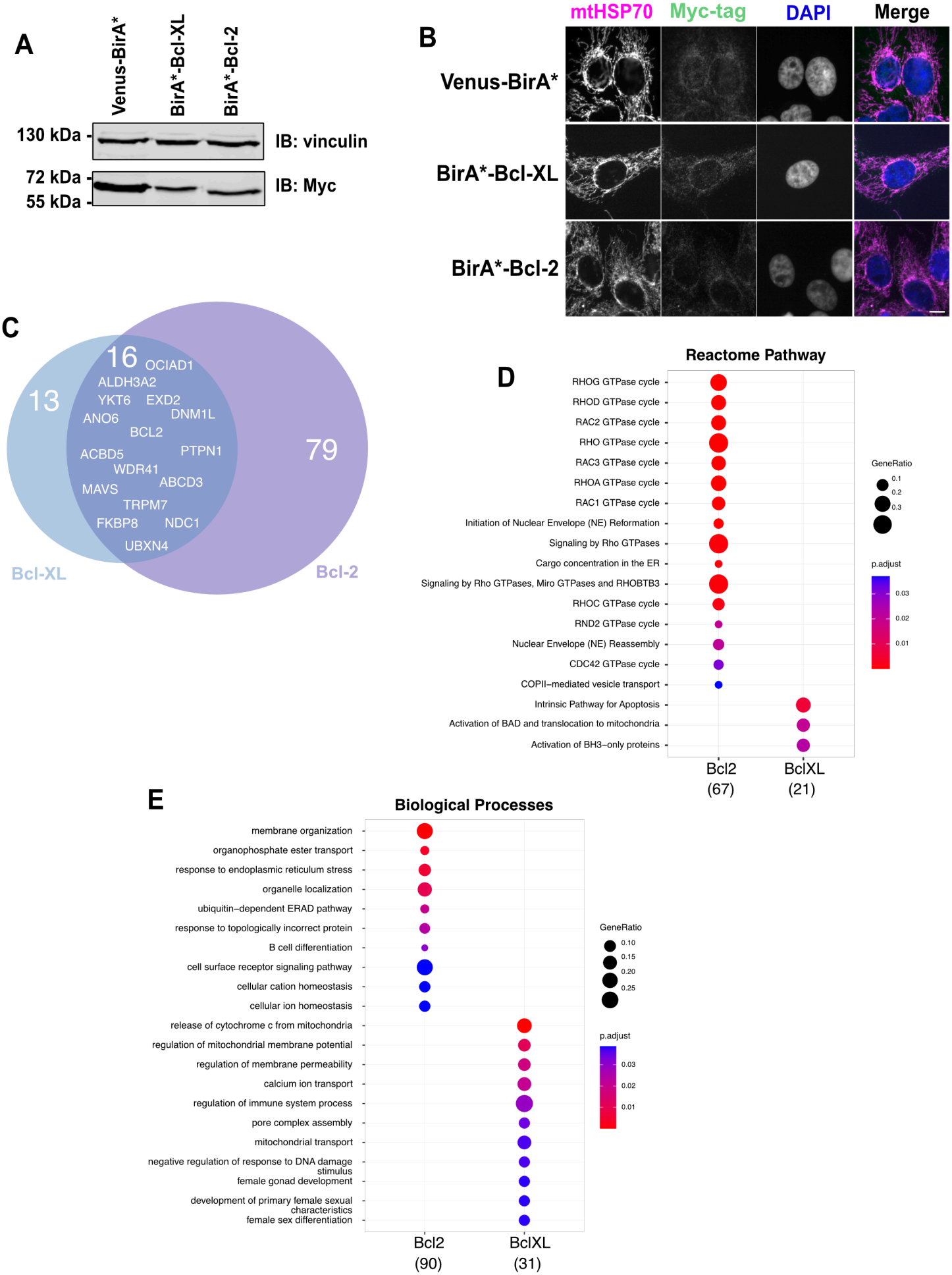
A
Venus-BirA*
BirA*-Bcl-XL
BirA*-Bcl-2
130 kDa
IB: vinculin
72 kDa
55 kDa
IB: Myc
B
mtHSP70
Myc-tag
DAPI
Merge
Venus-BirA*
BirA*-Bcl-XL
BirA*-Bcl-2
C
16
OCIAD1
ALDH3A2
YKT6
EXD2
ANO6
DNM1L
BCL2
ACBD5
PTPN1
WDR41
ABCD3
MAVS
TRPM7
FKBP8
NDC1
UBXN4
13
79
Bcl-XL
Bcl-2
D
Reactome Pathway
RHOG GTPase cycle
RHOD GTPase cycle
RAC2 GTPase cycle
RHO GTPase cycle
RAC3 GTPase cycle
RHOA GTPase cycle
RAC1 GTPase cycle
Initiation of Nuclear Envelope (NE) Reformation
Signaling by Rho GTPases
Cargo concentration in the ER
Signaling by Rho GTPases, Miro GTPases and RHOBTB3
RHOC GTPase cycle
RND2 GTPase cycle
Nuclear Envelope (NE) Reassembly
CDC42 GTPase cycle
COPII–mediated vesicle transport
Intrinsic Pathway for Apoptosis
Activation of BAD and translocation to mitochondria
Activation of BH3–only proteins
Bcl2
(67)
BclXL
(21)
GeneRatio
0.1
0.2
0.3
p.adjust
0.03
0.02
0.01
E
Biological Processes
membrane organization
organophosphate ester transport
response to endoplasmic reticulum stress
organelle localization
ubiquitin–dependent ERAD pathway
response to topologically incorrect protein
B cell differentiation
cell surface receptor signaling pathway
cellular cation homeostasis
cellular ion homeostasis
release of cytochrome c from mitochondria
regulation of mitochondrial membrane potential
regulation of membrane permeability
calcium ion transport
regulation of immune system process
pore complex assembly
mitochondrial transport
negative regulation of response to DNA damage stimulus
female gonad development
development of primary female sexual characteristics
female sex differentiation
Bcl2
(90)
BclXL
(31)
GeneRatio
0.10
0.15
0.20
0.25
p.adjust
0.03
0.02
0.01

Figure S2

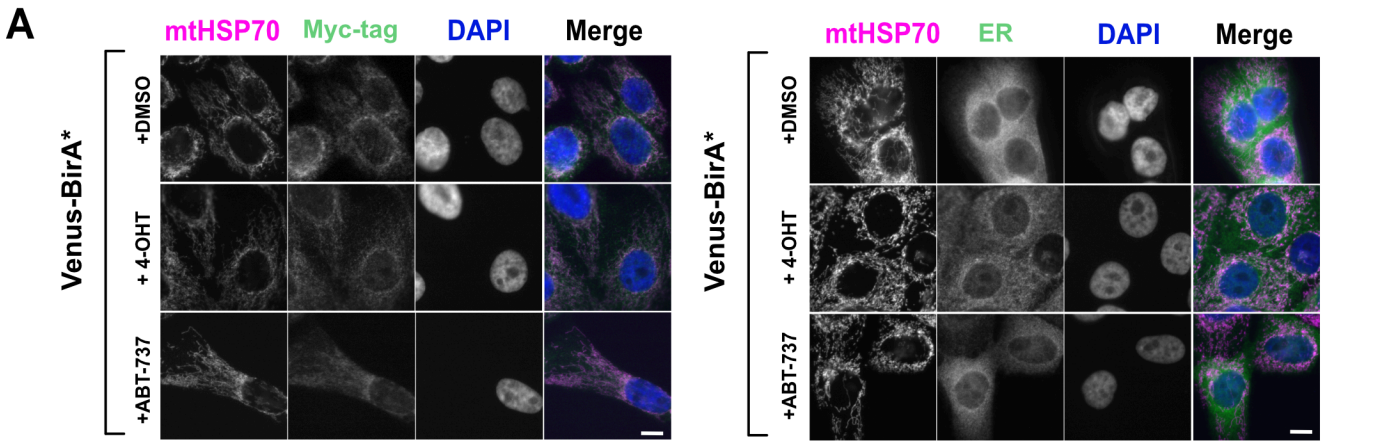

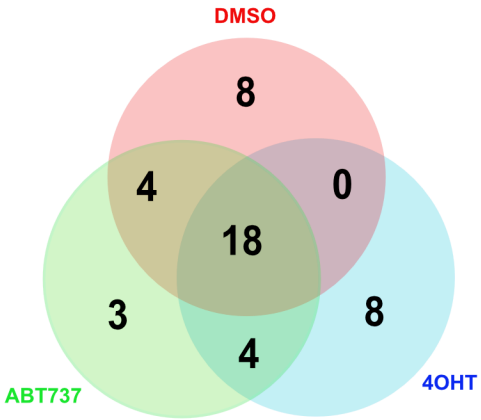

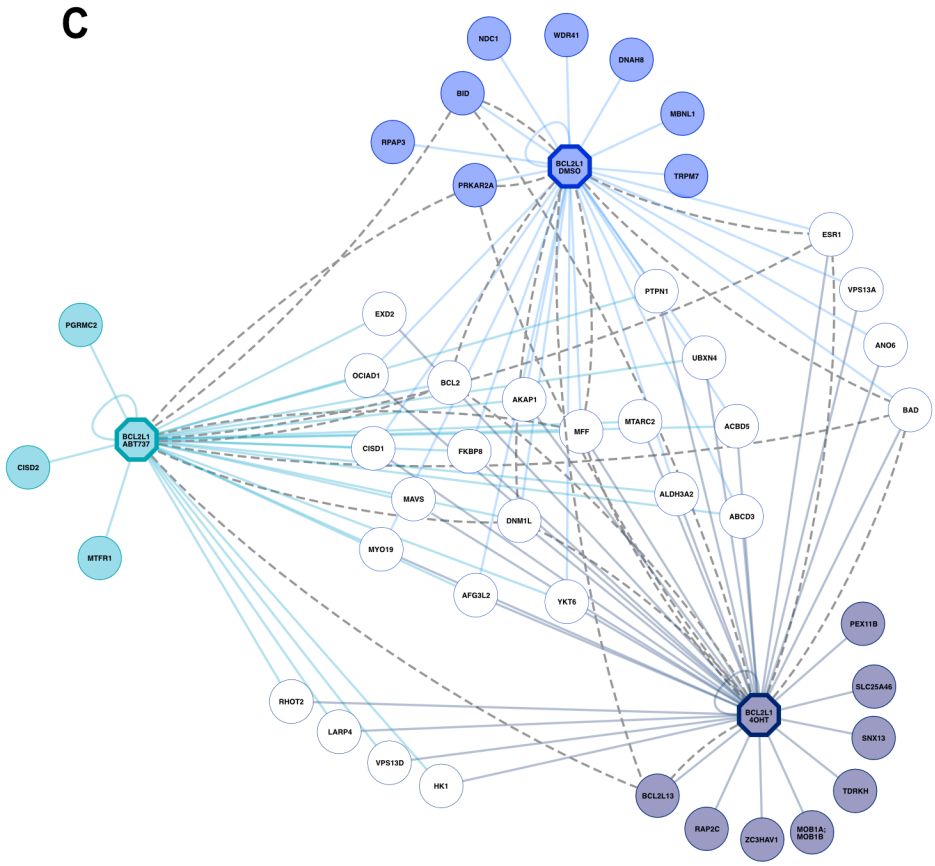

Bcl-XL STRING-predicted connections mapped

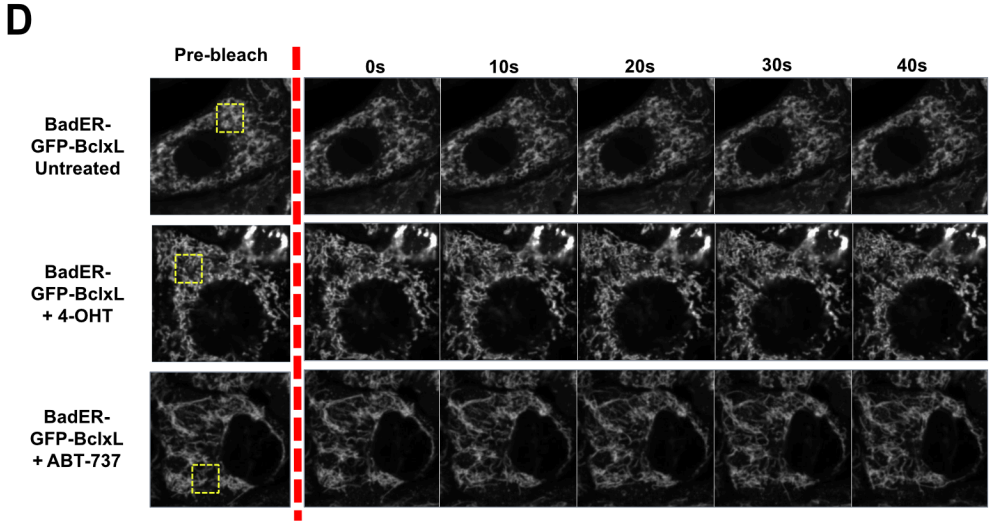

Figure S3

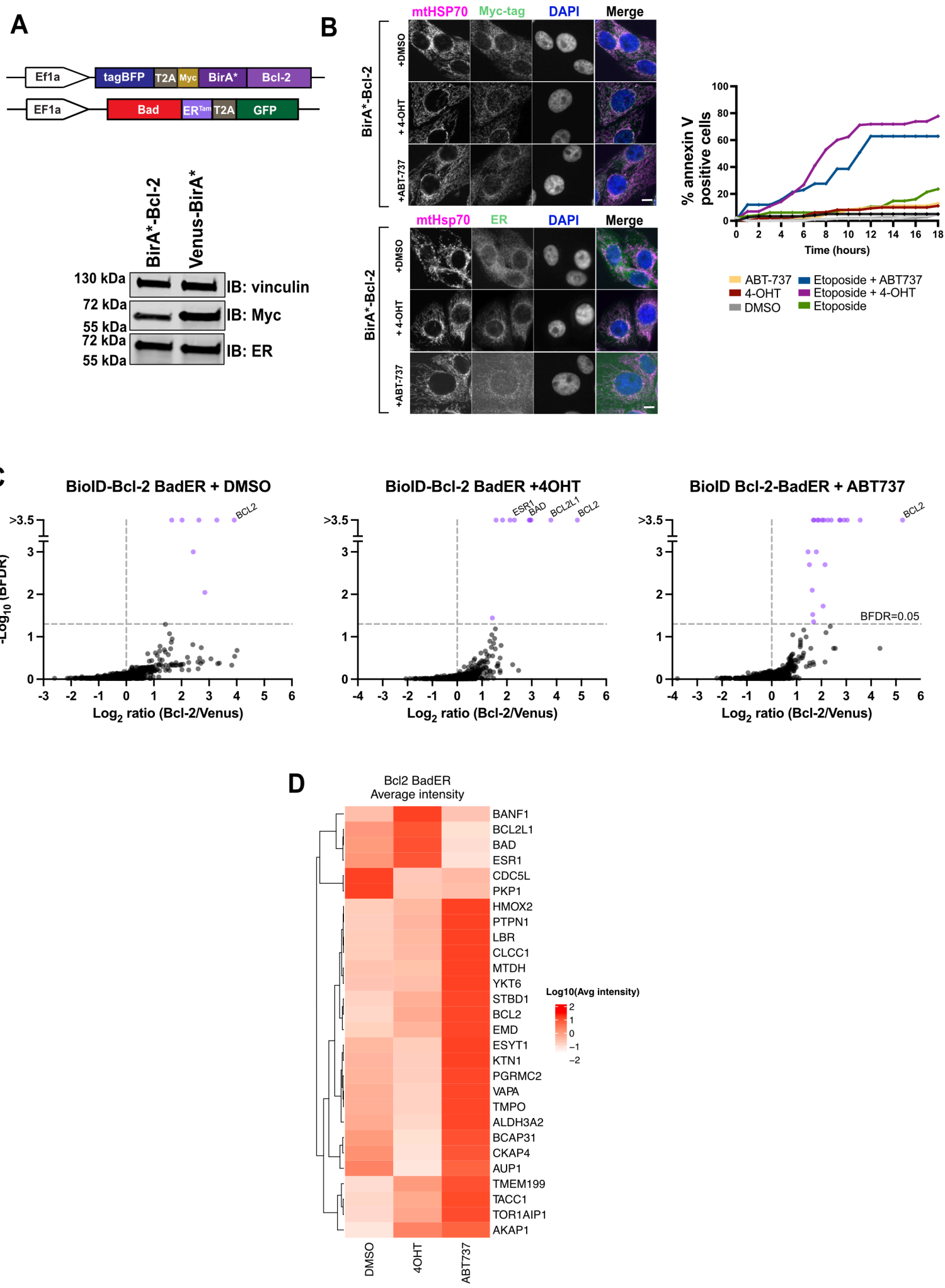
A
Ef1a
tagBFP
T2A
Myc
BirA*
Bcl-2
EF1a
Bad
ER^Tam
T2A
GFP
BirA*-Bcl-2
Venus-BirA*
130 kDa
IB: vinculin
72 kDa
55 kDa
IB: Myc
72 kDa
55 kDa
IB: ER
B
mtHSP70
Myc-tag
DAPI
Merge
BirA*-Bcl-2
+DMSO
+ 4-OHT
+ABT-737
mtHsp70
ER
DAPI
Merge
BirA*-Bcl-2
+DMSO
+ 4-OHT
+ABT-737
% annexin V positive cells
Time (hours)
ABT-737
4-OHT
DMSO
Etoposide + ABT737
Etoposide + 4-OHT
Etoposide
C
BioID-Bcl-2 BadER + DMSO
BioID-Bcl-2 BadER +4OHT
BioID Bcl-2-BadER + ABT737
-Log10 (BFDR)
Log2 ratio (Bcl-2/Venus)
BCL2
ESR1
BAD
BCL2L1
BFDR=0.05
D
Bcl2 BadER
Average intensity
BANF1
BCL2L1
BAD
ESR1
CDC5L
PKP1
HMOX2
PTPN1
LBR
CLCC1
MTDH
YKT6
STBD1
BCL2
EMD
ESYT1
KTN1
PGRMC2
VAPA
TMPO
ALDH3A2
BCAP31
CKAP4
AUP1
TMEM199
TACC1
TOR1AIP1
AKAP1
DMSO
4OHT
ABT737
Log10(Avg intensity)

Figure S4

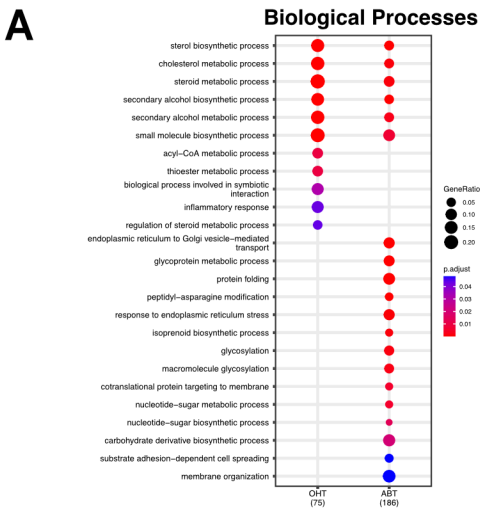
A
Biological Processes
sterol biosynthetic process
cholesterol metabolic process
steroid metabolic process
secondary alcohol biosynthetic process
secondary alcohol metabolic process
small molecule biosynthetic process
acyl−CoA metabolic process
thioester metabolic process
biological process involved in symbiotic interaction
inflammatory response
regulation of steroid metabolic process
endoplasmic reticulum to Golgi vesicle−mediated transport
glycoprotein metabolic process
protein folding
peptidyl−asparagine modification
response to endoplasmic reticulum stress
isoprenoid biosynthetic process
glycosylation
macromolecule glycosylation
cotranslational protein targeting to membrane
nucleotide−sugar metabolic process
nucleotide−sugar biosynthetic process
carbohydrate derivative biosynthetic process
substrate adhesion−dependent cell spreading
membrane organization
OHT (75)
ABT (186)
GeneRatio
0.05
0.10
0.15
0.20
p.adjust
0.04
0.03
0.02
0.01

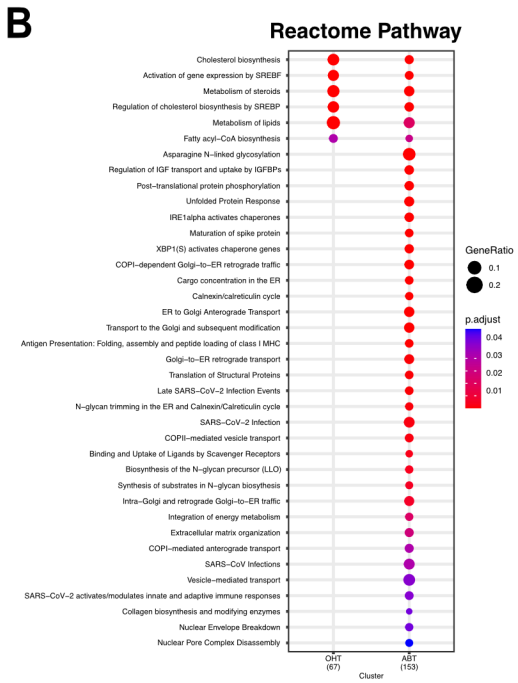
B
Reactome Pathway
Cholesterol biosynthesis
Activation of gene expression by SREBF
Metabolism of steroids
Regulation of cholesterol biosynthesis by SREBP
Metabolism of lipids
Fatty acyl−CoA biosynthesis
Asparagine N−linked glycosylation
Regulation of IGF transport and uptake by IGFBPs
Post−translational protein phosphorylation
Unfolded Protein Response
IRE1alpha activates chaperones
Maturation of spike protein
XBP1(S) activates chaperone genes
COPI−dependent Golgi−to−ER retrograde traffic
Cargo concentration in the ER
Calnexin/calreticulin cycle
ER to Golgi Anterograde Transport
Transport to the Golgi and subsequent modification
Antigen Presentation: Folding, assembly and peptide loading of class I MHC
Golgi−to−ER retrograde transport
Translation of Structural Proteins
Late SARS−CoV−2 Infection Events
N−glycan trimming in the ER and Calnexin/Calreticulin cycle
SARS−CoV−2 Infection
COPII−mediated vesicle transport
Binding and Uptake of Ligands by Scavenger Receptors
Biosynthesis of the N−glycan precursor (LLO)
Synthesis of substrates in N−glycan biosythesis
Intra−Golgi and retrograde Golgi−to−ER traffic
Integration of energy metabolism
Extracellular matrix organization
COPI−mediated anterograde transport
SARS−CoV Infections
Vesicle−mediated transport
SARS−CoV−2 activates/modulates innate and adaptive immune responses
Collagen biosynthesis and modifying enzymes
Nuclear Envelope Breakdown
Nuclear Pore Complex Disassembly
OHT (67)
ABT (153)
Cluster
GeneRatio
0.1
0.2
p.adjust
0.04
0.03
0.02
0.01

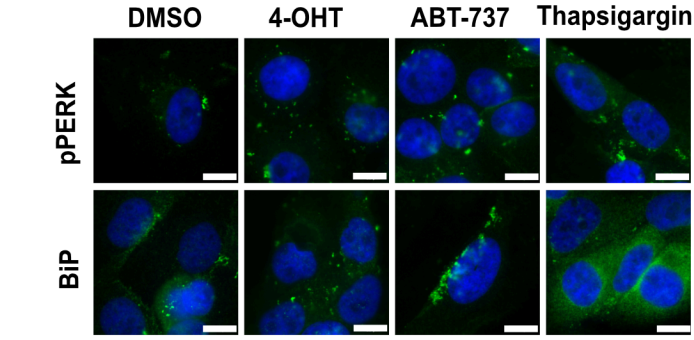
C
DMSO
4-OHT
ABT-737
Thapsigargin
pPERK
BiP

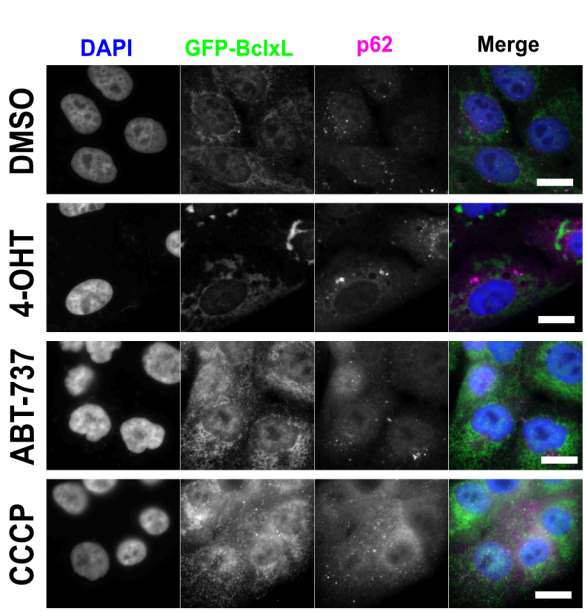
D
DAPI
GFP-BclxL
p62
Merge
DMSO
4-OHT
ABT-737
CCCP

Figure S5

Full length western blots

A.

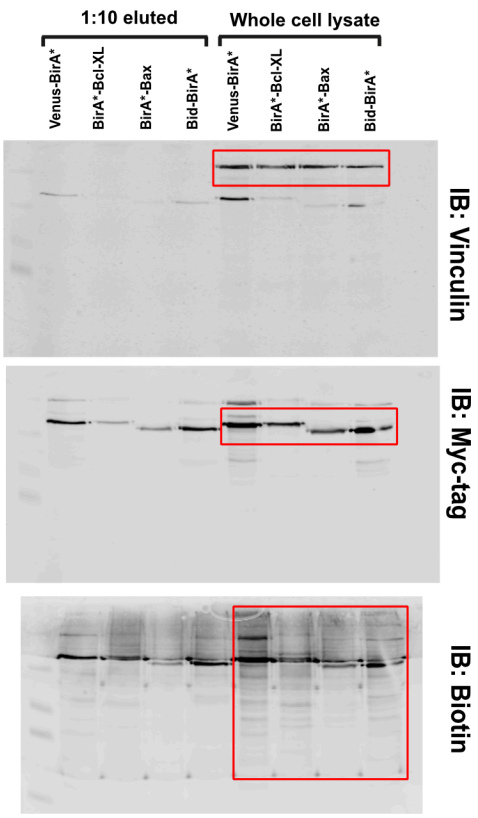

Figure 1C

B.

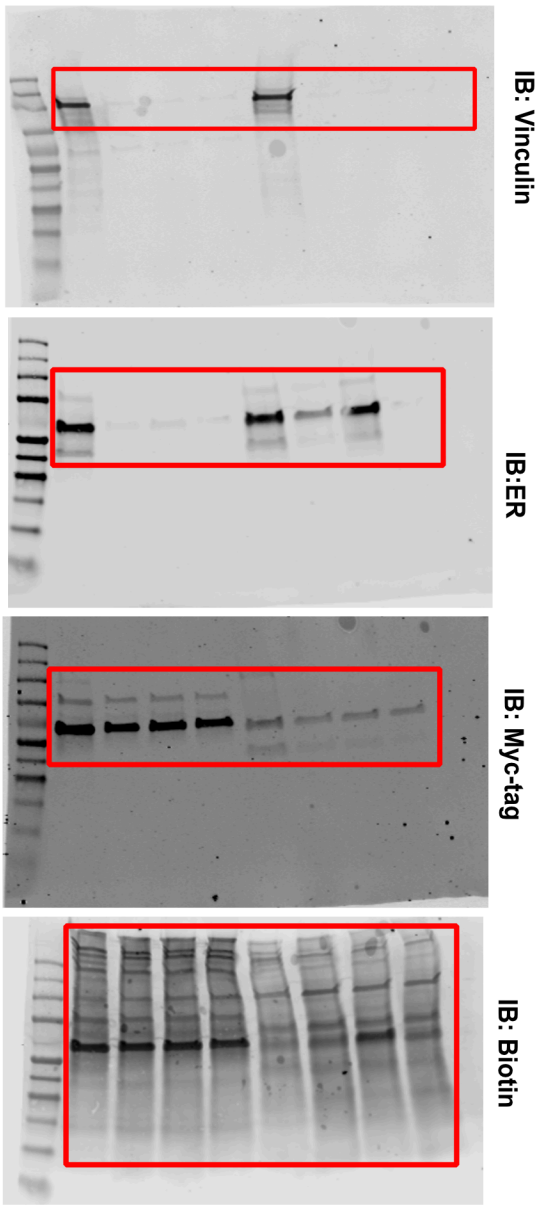

Figure 4D

C.

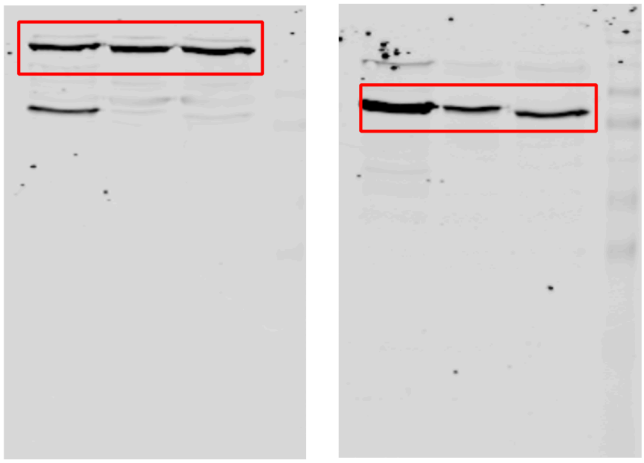

Figure S2B

D.

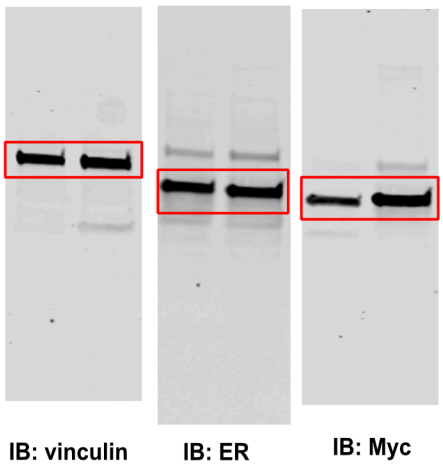

Figure S5B

Figure S6

Details of proteomics data sets in PRIDE.

PXD058099 – BioID data related to Figure 1. MCF10A cells expressing BAX, BID, BCL-XL and Venus BirA* fusions.

PXD058123 – BioID data related to Figure S1, with MCF10A cells expressing BAX-WT, BAX-S184V and Venus BirA* fusions.

PXD058132 – BioID data related to Figures 2, S2, S3 and 4. Data from MCF10A cells expressing BCL-XL and Venus BirA* fusions along with BadER, treated with DMSO, ABT-737 and 4-OHT treatments, and MCF10A cells expressing BCL-2 BirA* fusion.

PXD058179 – BioID data related to Figure S4, with MCF10A cells expressing BCL-2 and Venus BirA* fusions along with BadER and treated with DMSO, ABT-737 and 4-OHT.

PXD058181 – Proteomics data related to Figure 5 F, G and H. This includes mass spectrometry data from whole cell lysates of MCF10A cells expressing BadER and BirA*-BCL-XL, treated with DMSO, ABT-737 or 4-OHT.